BRITISH JOURNAL OF HOSPITAL MEDICINE

ARTICLE

Preoperative Prediction of Her-2 and Ki-67 Status in Gastric Cancer Using ^{18}F-FDG PET/CT Radiomics Features of Visceral Adipose Tissue

Demei Chen[1], Rui Zhou[1], Bo Li[1,*]

[1]Department of Nuclear Medicine, Chongqing University Cancer Hospital, Chongqing, China
*Correspondence: lb12sunxixi@163.com (Bo Li)

Abstract

Aims/Background Immunohistochemistry (IHC) is the main method to detect human epidermal growth factor receptor 2 (Her-2) and Ki-67 expression levels. However, IHC is invasive and cannot reflect their expression status in real-time. This study aimed to build radiomics models based on visceral adipose tissue (VAT)'s ^{18}F-fluorodeoxyglucose (^{18}F-FDG) positron emission tomography/computed tomography (PET/CT) imaging, and to evaluate the relationship between radiomics features of VAT and positive expression of Her-2 and Ki-67 in gastric cancer (GC).

Methods Ninety patients with GC were enrolled in this study. ^{18}F-FDG PET/CT radiomics features were calculated using the PyRadiomics package. Two methods were employed to reduce radiomics features. The machine learning models, logistic regression (LR), and support vector machine (SVM), were constructed and estimated by the receiver operator characteristic (ROC) curve. The correlation of outstanding features with Ki-67 and Her-2 expression status was evaluated.

Results For the Ki-67 set, the area under of the receiver operator characteristic curve (AUC) and accuracy were 0.86 and 0.79 for the LR model and 0.83 and 0.69 for the SVM model. For the Her-2 set, the AUC and accuracy were 0.84 and 0.86 for the LR model and 0.65 and 0.85 for the SVM model. The LR model for Ki-67 exhibited outstanding prediction performance. Three wavelet transform features were correlated with Her-2 expression status (p all < 0.001), and one wavelet transform feature was correlated with the expression status of Ki-67 ($p = 0.042$).

Conclusion ^{18}F-FDG PET/CT-based radiomics models of VAT demonstrate good performance in predicting Her-2 and Ki-67 expression status in patients with GC. Radiomics features can be used as imaging biomarkers for GC.

Key words: machine learning; radiomics; ^{18}F-FDG PET/CT; visceral adipose tissue; human epidermal growth factor receptor 2 (Her-2); Ki-67; gastric cancer (GC)

Submitted: 18 June 2024 Revised: 20 July 2024 Accepted: 31 July 2024

How to cite this article:
Chen D, Zhou R, Li B. Preoperative Prediction of Her-2 and Ki-67 Status in Gastric Cancer Using ^{18}F-FDG PET/CT Radiomics Features of Visceral Adipose Tissue. Br J Hosp Med. 2024. https://doi.org/10.12968/hmed.2024.0350.

Introduction

Gastric cancer (GC) is a common malignant gastrointestinal tumor with the fifth-largest incidence and mortality rate in the world (Bray et al, 2024). In 2022, there were more than 968,000 new cases and 660,000 deaths causing by GC. Although targeted therapies are currently available for treatment of GC, the survival rate for late-stage GC remains low (Smyth et al, 2020), due to low early diagnosis rates, a lack of effective biological and behavioral predictors, and low treatment rates for GC. Early diagnosis and understanding of the molecular biology of GC, as

well as the discovery of sensitive biological markers, are crucial for timely and effective diagnosis and treatment. Current treatment options are chosen mainly based on indicators such as clinical phase, pathological type, human epidermal growth factor receptor 2 (Her-2), Ki-67, and other conditions (Zhang et al, 2023).

Ki-67 is widely recognized as a cell proliferation marker, providing an objective reflection of tumor cell growth and demonstrating significant clinical value. Elevated Ki-67 levels are indicative of increased cell proliferation activity, which has been closely linked to lower survival rates and a poor prognosis for patients with GC (Awadh et al, 2023; Li et al, 2015). Her-2 is a receptor-like protein encoded by *Her-2* (human epidermal growth factor receptor 2) gene. It is abnormally activated when exposed to certain stimuli, and it plays a crucial role in regulating cell proliferation, apoptosis, tumor angiogenesis, and metastasis through multiple signaling pathways (Roviello et al, 2022). The positivity rate of Her-2 in patients with GC ranges from 6% to 29.5% (Boku, 2014), and its expression often indicates an unfavorable prognosis. Currently, the "biopsy" method is considered the gold standard for diagnosing the expression status of Her-2 and Ki-67, which can guide subsequent treatment strategies for GC patients. However, biopsy presents challenges as an invasive procedure conducted via endoscopy or surgery to collect tissue samples for analysis. It may not always provide sufficient tissue, resulting in missed and misdiagnosed cases and potentially inaccurate or undetectable results (Le Berre et al, 2020). This invasive approach also carries the risk of pain, bleeding, and postoperative infection (Abrahao-Machado and Scapulatempo-Neto, 2016; Levy and Gralnek, 2016). Additionally, some patients may experience anxiety about undergoing endoscopy, leading to delayed examination. Surgical exploration can impose significant financial burdens and surgical risks on patients. Furthermore, subjective differences in observers' interpretations could impact the assessment of Her-2 and Ki-67. Therefore, a non-invasive method is urgently needed to avoid the risk of invasive tests.

The radiological examination is a non-invasive and reproducible modality that enables a comprehensive evaluation of tumors, including their relationship with surrounding tissue structures. It provides qualitative and quantitative detection of tumor occurrence, development, and treatment response (Orăşeanu et al, 2023). Building upon the foundation of Computer Aided Diagnosis, researchers have incorporated big data technology, leading to the development of radiomics. Radiomics can deeply mine a large number of high-dimensional data through mathematical methods and maximize the use of radiological images (computed tomography [CT], magnetic resonance imaging [MRI], ultrasound, positron emission tomography [PET]) (Tomaszewski and Gillies, 2021). Quantitative features reveal information on genetic and protein expression profiles of tumors, which radiologists cannot obtain with the naked eye. Radiomics can comprehensively reproduce the pathophysiological process of tumors in real time and indicate many imaging biomarkers (Tunali et al, 2021). It can be helpful in cancer diagnosis, detection, and prognostic evaluation, and to predict the treatment response and monitor disease progression (Pan et al, 2023). Radiomics indicates imaging biomarkers for the expression of Her-2

and Ki-67, and researchers utilize radiomics to predict the expression of Her-2 and Ki-67 in breast cancer (Acar et al, 2019), brain gliomas (Moon et al, 2023), and other diseases.

Some previous studies used CT radiomics features (Ma et al, 2022a; Zhao et al, 2023) or PET/CT radiomics features (Jiang et al, 2024; Liu et al, 2023; Qin et al, 2024) of GC tumors to predict Her-2 expression. Radiomics features derived from PET/CT images can suggest information about the metabolism of biological tissues compared with features derived from CT and MRI images. However, there is heterogeneity in the metabolism of different GC pathological types, and not all malignant GCs have high fluorodeoxyglucose (FDG) uptake. For example, low-adherent carcinomas (including signet ring cell carcinomas and mucinous adenocarcinomas) have low ^{18}F-FDG uptake and often display hypometabolism on imaging compared with adenocarcinoma (Dondi et al, 2021). Therefore, the radiomics features of tumors cannot accurately reflect their pathological characteristics.

Visceral adipose tissue (VAT) plays an important role in the development and prognosis of GC (Lee et al, 2020). Previous studies have found that CT attenuation and metabolism of VAT can evaluate and predict the clinical T stage (Ma et al, 2022b) and prognosis of GC patients (Lee et al, 2020; Lu et al, 2022). It is well known that VAT is closely related to the occurrence of malignant tumors, and adipocytes participate in the proliferation and invasion of cancer cells through release of proinflammatory cytokines and cancer-related adipocytokines (Avgerinos et al, 2019; Martin-Perez et al, 2022).

VAT volume, CT attenuation, FDG metabolism, and pathological indicators (Ki-67 and Her-2) can be used to evaluate the prognosis of GC. Thus, associations among abnormal changes in these indices are worth exploring. This study aims to test the predictive value of radiomics features of VAT for Ki-67 and Her-2 status in GC patients.

Methods

Patients

From January 2019 to December 2022, 90 patients with GC confirmed by pathology, and with complete clinical data and ^{18}F-FDG PET/CT imaging data, were retrospectively enrolled. Inclusion criteria: (1) GC patients confirmed by pathology; (2) Patients who underwent abdominal PET/CT examination within 2 weeks before surgery; (3) Patients that had not received any chemoradiotherapy, targeted therapy, or immunotherapy before admission; (4) Immunohistochemistry (IHC) and fluorescence *in situ* hybridization (FISH) if required were performed. Exclusion criteria: (1) History of other malignant tumors; (2) Multiple tumors occurring at the same time; (3) History of abdominal surgery; (4) Incomplete clinical data; (5) The stomach was underfilled due to inadequate drinking water before PET/CT examination; (6) The image did not meet the post-processing standards (Fig. 1). This study was conducted in accordance with the Declaration of Helsinki and approved by the Medical Ethics Committee of Chongqing University Cancer Hospital (ethics number: CZLS2024006-A). As this study is a retrospective study,

all data included in the research are sourced from our hospital's big data platform, and all examinations were part of normal diagnosis and treatment during patients' hospitalization. Because there was no harm in interests or privacy of the patients in this study, the Medical Ethics Committee of Chongqing University Cancer Hospital waived the need for informed consent during ethical review.

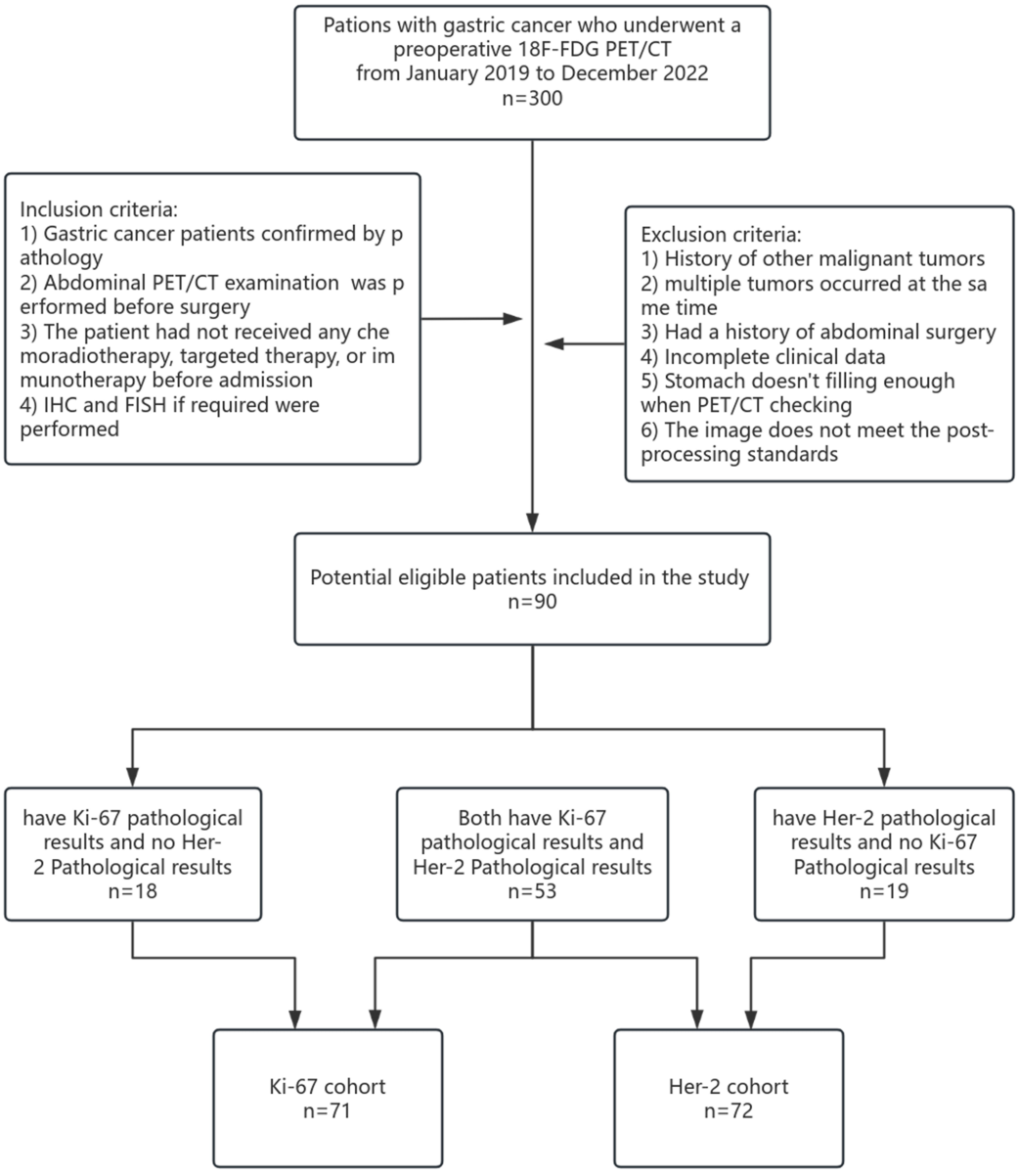

Fig. 1. Flowchart of the study cohort selection. ^{18}F-FDG, ^{18}F-fluorodeoxyglucose; PET/CT, positron emission tomography/computed tomography; IHC, immunohistochemistry; FISH, fluorescence *in situ* hybridization; Her-2, human epidermal growth factor receptor 2.

^{18}F-FDG PET/CT Scan

Patients underwent ^{18}F-FDG PET/CT scanning with the use of a whole-body PET/CT scanner (GE Healthcare, Discovery 710). Patients fasted for at least 6 hours before the scan to achieve fasting blood glucose $<$11.1 mmol/L. After rest-

ing for 20 minutes, ^{18}F-FDG radiotracer was administered intravenously (approximately 0.08–0.1 mCi/kg). Patients were then placed in a dark room for 40–60 minutes. Before entering the examination room, patients emptied their bladder and filled the stomach with 800–1000 mL of water. During the scanning, patients were supine with their hands crossed over their heads. The scan encompassed the crown of the head to mid-thigh. CT images were obtained by helical volume scanning with the following parameters: tube voltage = 120 kV, current = 180 mA, detector coverage = 40 mm, pitch = 0.984:1, rotation = 0.6 s, coverage speed = 65.62 mm/s, coverage time = 15.6 s, field of view (FOV) = 70.0 cm, helical slice thickness = 3.75 mm, window width = 400 Hounsfield units (HU), window level = 40 HU, reconstruction slice thickness = 1.25 mm, interlamellar spacing = 0.625 mm. The images were reconstructed by 30% adaptive statistical iterative reconstruction (ASiR). Three-dimensional PET collection was obtained by step scanning and other parameters were 1.5 min/bed, 7–8 beds/person, overlap = 11 mm, FOV = 70 cm. The PET image was reconstructed using a combination of three algorithms, namely filtered back projection, time of flight, and the ordered subset expectation maximization with 2 iterations, 24 subsets, matrix size of 192 × 192, and a filter cut-off of 6.4 mm. Attenuation correction was performed on PET images using CT data, and fusion images were obtained.

The Detection of Ki-67 and Her-2 Expression in Lesions

The Ki-67 labeling index and Her-2 status were evaluated by immunohistochemistry (IHC) and quantified by a pathologist in all patients. The result derived from the resection specimen was accepted when the discordance between endoscopy and resection for Her-2 status was detected; the optimal threshold value of Ki-67 had not yet been identified. According to studies in this country and abroad, expression in normal tissues and benign tumors is usually less than 10%, and for high malignant tumors is usually more than 50%. Patients were divided into low-expression (<50%) and high-expression groups (≥50%) according to the pathological report of our hospital. The expression level of Her-2 was detected by IHC (and fluorescence *in situ* hybridization (FISH), if required). Positive Her-2 expression was defined as 3+ on IHC, or 2+ on IHC with positive FISH. Negative Her-2 expression was defined as 0, 1+ on IHC, or 2+ on IHC and negative FISH.

VAT Data Processing

Segmentation, Radiological Characteristics, and Radiomics Features Extraction of VAT

The region of interest (ROI) in the VAT was segmented by the 3D slicers software (Version 5.4, Surgical Planning Laboratory, Brigham and Women's Hospital Harvard Medical School, Boston, MA, USA), and the radiomics features were extracted by PyRadiomics (Version 3.0.1, Dana-Farber Cancer Institute, Brigham and Women's Hospital Harvard Medical School, Boston, MA, USA) in Python (version 3.7, Python Software Foundation). The reference manual for open-source Python packages, including the machine learning (ML) repository, accords with the image biomarkers standardization initiative. The CT value threshold of VAT was set be-

tween –150 and –50 HU, and the ROI was derived from the range 7.5 mm up and 7.5 mm down from the central level of lumbar vertebra2-lumbar vertebra3. The ROI was delineated along the abdominal wall layer by layer (Fig. 2). The CT attenuation (unit: HU) and volume (unit: cm × cm × cm) of ROI were measured. The ROI was matched to the PET image, obtaining Standardized Uptake Value (SUV), including maximum SUV (SUVmax) and average SUV (SUVmean), value. Areas of physiological FDG activity in the urine, intestine, and blood vessels were avoided when the ROI was delineated. ROIs of VAT as well as PET images were then extracted and saved, and subsequently they were imported into PyRadiomics. Before feature extraction, image gray normalization and a discretization process with a fixed bin width of 0.25 were performed, followed by resampling to voxel dimensions of 3 × 3 × 3 mm^3. The remaining parameters were initialized with the default values provided by PyRadiomics. The extracted features included three groups: first-order statistics features (n = 18), second-order statistics features (n = 75), and higher-order statistical features (n = 744). First-order statistical features included the mean intensity, standard deviation, skewness, kurtosis, and entropy of the image voxels. These values provide a description of the intensity distribution histogram of the image voxels. Second-order statistical features enable spatial arrangement by describing statistical interrelationships between adjacent voxels through multiple matrices. For example, the gray-level co-occurrence matrix (GLCM) reflects the probability of voxel values occurring at a given direction and distance, the Gray Level Run Length Matrix (GLRLM) describes the length of consecutively occurring voxels of the same gray level in a given direction, the Gray Level Size Zone Matrix (GLSZM) quantizes the region of continuous voxel values in an image, and the Gray Level Dependence Matrix (GLDM) measures the difference between adjacent voxels based on voxel values. High-level features are mainly based on wavelet transformation which includes eight main transformations (namely: HLL, LLL, HLH, HHL, LLH, LHH, LHL and HHH). The first-order statistics features and second-order statistics features were both extracted from each transformed image (Fig. 2).

Feature Reduction, Model Construction and Evaluation

The scikit-learn (sklearn) package (Version 1.0.2, https://scikit-learn.org) in Python version 3.9 was used for feature reduction and model construction. Twenty patients were randomly selected to calculate the intraclass correlation coefficient (ICC), and the ROI was delineated by another radiologist. Features with ICC >0.75 were considered to be highly reproducible, and were included in the next stage of the analysis. Feature reduction included the following steps: firstly, missing values of each feature were first replaced by median values, and then values of each feature were standardized by the formula: $\chi_{new} = \frac{\chi-\mu}{\sigma}$ (μ is the mean of the features and σ is the standard deviation of the features). Finally, the feature dimensionality was reduced, and the most relevant features were selected to build the model. In the first step, Recursive Feature Elimination (RFE) was used, and the algorithm was set to remove two features per iteration, ultimately retaining the best 15 features (the logistic regression (LR)-RFE model and the support vector machine (SVM)-RFE model were used to identify important features). In the second step,

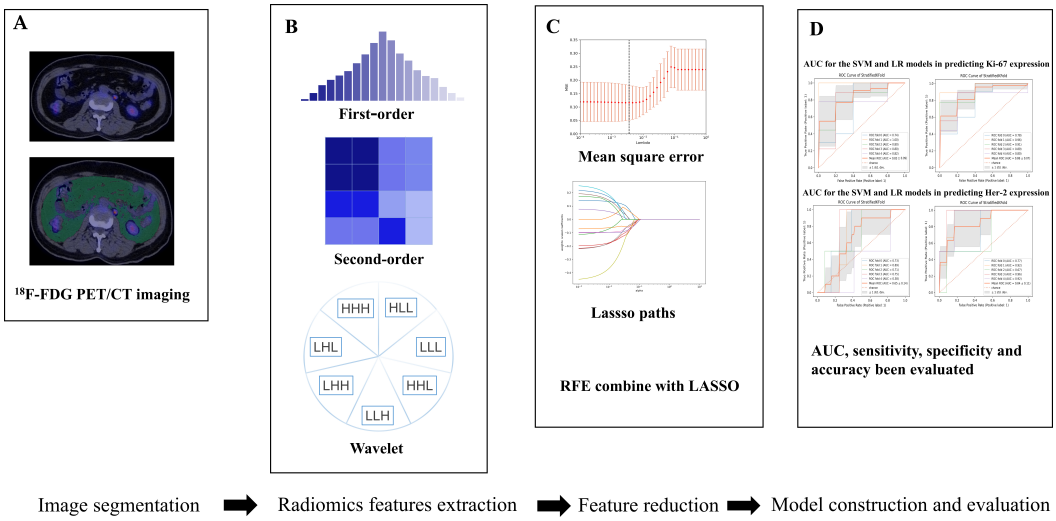

Fig. 2. The pipeline of the study. (A) Data preprocessing and segmentation of visceral adipose tissue (VAT). (B) Radiomic features of VAT were extracted based on images of positron emission tomography (PET). (C) The support vector machine (SVM)-Recursive Feature Elimination (RFE), logistic regression (LR)-RFE and the least absolute shrinkage and selection operator (LASSO) algorithm were used for feature reduction. (D) The diagnostic performance of models was evaluated by the sensitivity, specificity, accuracy and the area under of the receiver operator characteristic curve (AUC).

the least absolute shrinkage and selection operator (LASSO) with 10-fold cross-validation were used to select optimal features from the 15 radiomics features. The parameters were initialized with the default values (Fig. 3). Using the five-fold cross-validation method, the LR (regularization parameter is L2, solver is liblinear, the maximum number of iterations is 1000) and SVM (the kernel function is radial basis function) ML models were constructed. The basic idea of RFE is to recursively retain the features that are most important to a preset classifier (such as SVM, LR) in successive iterations until a preset number of features is reached. LASSO is a linear regression method, the basic principle of which is to introduce L1 regularization term on the basis of ordinary least squares method and realize the feature selection of the model by minimizing the objective function.

Use the area under of the receiver operator characteristic curve (AUC), sensitivity, specificity and accuracy to quantify different models' performance (Fig. 2).

Statistical Analyses

SPSS 25.0 software (IBM Corp, Armonk, NY, USA) was for statistical analysis. The Shapiro-Wilk was employed to examine the measurement data. Normally distributed data were expressed as Mean $\pm$ SD, and the independent sample *t*-test was utilized for comparison between the groups. Non-normally distributed data were reported as Median (First quartile, Third quartile) using the quartile technique, and the Mann-Whitney U test was used to examine group differences. Count data were expressed as (n (%)), and associations between the groups were assessed using the χ^2 test. The correlations between optimal features and the state of Ki-67 and Her-2 of GC patients were assessed. Point-biserial correlation was performed for

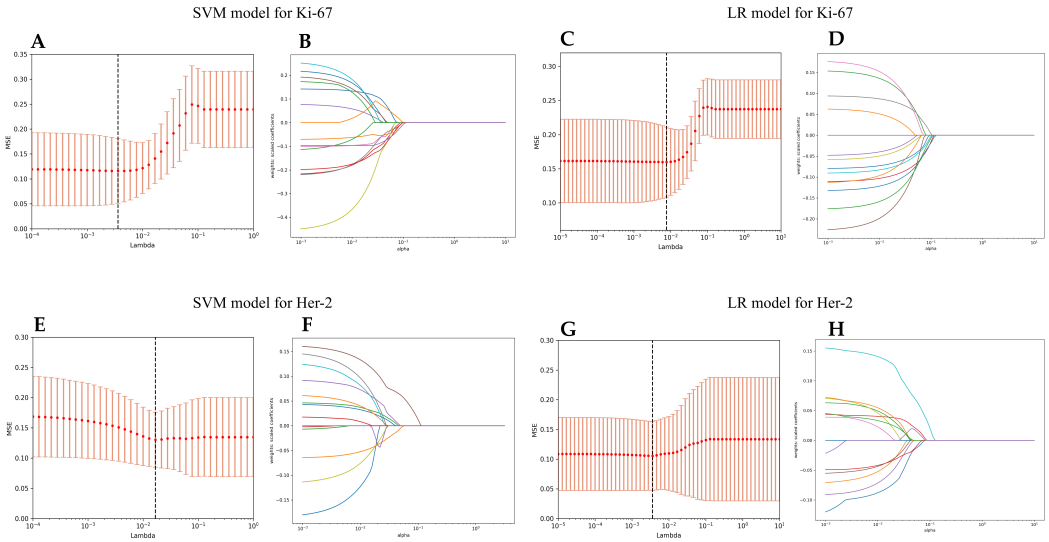

Fig. 3. The LASSO algorithm and 10-fold cross-validation were used to extract the optimal subgroup of radiomics features in four models. (A,C,E,G) The mean square error (MSE) varies with the value of lambda; the black vertical bar represents the value of lambda when the model fits best. (B,D,F,H) The penalty diagram of the coefficient of radiomics features.

normally distributed data, whereas the Kruskal-Wallis test was performed for non-normally distributed data. Two-tailed p values < 0.05 were considered statistically significant.

Results

Basic Information

The study included 90 patients with GC, including 49 men and 41 women, with an age range of 24 to 80 years and an average age of 61.1 years. The Ki-67 set had 71 GC patients, including 25 low-expression patients and 46 high-expression patients. The Her-2 set had 72 GC patients, including 11 positive-expression patients and 61 negative-expression patients. There was a significant difference in CA199 between low Ki-67 and high Ki-67 groups, all other group differences in radiological and clinical characteristics were non-significant (Table 1).

Feature Reduction and Selection

For each patient, 837 features were extracted, features with excellent reproducibility (intra-/inter-observer ICCs >0.75) were used for subsequent radiomics analysis (Ki-67 analysis had 820 features and Her-2 analysis had 816 features). When the lambda value was $7.74 \times e^{-3}$, the 10-fold cross-validation LASSO method selected 14 features for the LR model of Ki-67, and when the lambda value was $3.59 \times e^{-3}$, 14 features were chosen for the SVM model of Ki-67. When the lambda value was $3.59 \times e^{-3}$, the 10-fold cross-validation LASSO method selected 13 features for the LR model of Her-2, and when the lambda value was $1.67 \times e^{-3}$, 11 features were selected for the SVM model of Her-2. Fig. 3 and Table 2 show the screening process and detailed distribution of features.

Table 1. Radiological and clinical characteristics of the enrolled patients in the Ki-67 and Her-2 cohorts.

	Ki-67 set (n = 71)		$t/z/\chi^2$	p	Her-2 set (n = 72)		$t/z/\chi^2$	p
	Low (n = 25)	High (n = 46)			Positive (n = 11)	Negative (n = 61)		
Sex, (n)			1.862	0.172			0.469	0.493
Male	11	28			7	32		
Female	14	18			4	29		
Age (years), [median (Q25, Q75)]	58.00 (52.00, 68.50)	65.00 (51.00, 69.50)	–0.030	0.976	57.00 (52.00, 67.00)	61.00 (54.50, 70.00)	–0.697	0.486
BMI (kg/cm^2), [median (Q25, Q75)]	22.21 (19.73, 24.02)	21.76 (19.23, 24.54)	–0.283	0.777	20.58 (19.16, 25.08)	21.63 (19.35, 23.56)	–0.117	0.907
Tumor location, (n)			3.286	0.350			1.152	0.765
Stomachus cardiacus	3	12			1	13		
Stomachus body	8	16			5	20		
Stomachus pyloricus	13	15			4	22		
Multisite of stomach	1	3			1	6		
Differentiated degree, (n)			0.000	0.993			0.171	0.679
Well	6	11			1	12		
Poorly	19	35			10	49		
CEA, [median (Q25, Q75)]	1.60 (0.82, 3.15)	2.20 (1.16, 3.68)	–0.813	0.416	2.68 (1.55, 5.38)	1.60 (0.97, 3.29)	–1.331	0.183
CA125, [median (Q25, Q75)]	19.10 (7.05, 33.85)	9.70 (5.50, 23.35)	–1.109	0.267	10.10 (5.70, 24.60)	10.20 (5.90, 25.1)	–0.321	0.748
CA199, [median (Q25, Q75)]	29.52 (9.73, 124.02)	16.46 (8.28, 27.53)	–2.131	0.033	7.75 (1.46, 36.32)	19.24 (8.74, 31.19)	–1.417	0.157
CT-mean attenuation (HU), mean ± SD	–89.41 ± 7.89	–89.50 ± 8.75	0.045	0.964	–89.40 ± 8.88	–88.14 ± 8.90	0.431	0.668
VAT-volume (cm^3), [median (Q25, Q75)]	109.14 (55.46, 176.96)	81.27 (55.08, 189.41)	–0.445	0.656	74.67 (53.40, 192.83)	89.69 (37.41, 146.94)	–0.352	0.725
SUVmax, [median (Q25, Q75)]	2.48 (2.19, 2.69)	2.29 (2.00, 2.56)	–1.661	0.097	2.25 (2.02, 2.50)	2.28 (2.14, 2.60)	–0.587	0.557
SUVmean, [median (Q25, Q75)]	0.68 (0.59, 0.80)	0.69 (0.56, 0.83)	–0.036	0.971	0.71 (0.51, 0.83)	0.69 (0.57, 0.85)	–0.399	0.690

$p < 0.05$ is considered statistically significant. Mean (Q25, Q75), Median (First quartile, Third quartile); SD, standard deviation; Her-2, human epidermal growth factor receptor 2; BMI, Body Mass Index; Multisite of stomach, More than one site; SUVmax, maximum standardized uptake value; SUVmean, mean standardized uptake value; HU, Hounsfield units.

Table 2. The feature distribution of different screening methods.

Feature category	SVM-RFE+LASSO	LR-RFE+LASSO
	Number	Number
Ki-67		
First-order	1	0
Second-order	2	1
Wavelet transform	11	13
Her-2		
First-order	0	0
Second-order	1	2
Wavelet transform	10	11

Her-2, human epidermal growth factor receptor 2; SVM-RFE, support vector machine-Recursive Feature Elimination; LR-RFE, logistic regression-Recursive Feature Elimination; LASSO, least absolute shrinkage and selection operator.

Model Predictive Performance Assessment

Among the four predictive models, the Ki-67 model performed better than the Her-2 model, with AUC, accuracy, sensitivity, and specificity of 0.86, 0.79, 0.83, and 0.72 for the LR predictive model, and 0.83, 0.69, 0.99, and 0.18 for the SVM predictive model, respectively. The LR model performed better than the SVM predictive model not only for the Ki-67 set but also for the Her-2 set, and the LR model of Ki-67 had the most stable and optimum performance in all aspects. All model performances are presented in Table 3 and Fig. 4.

Analysis of Features Correlated with Ki-67 and Her-2

Some selected features were correlated with the state of Ki-67 and Her-2, with 1 second-order feature and 3 wavelet transform features associated with Her-2 expression (p = 0.045, 0.004 and 0.003, 0.003 respectively), and one wavelet transform feature related to the status of Ki-67 (Table 4).

Discussion

Numerous studies have demonstrated that VAT is linked to the prognosis, clinical stage, and bioindicators of various tumors (Matsui et al, 2022; Ma et al, 2022b; Lu et al, 2022; Lee et al, 2020). However, the relationship between VAT metabolism and gastrointestinal cancer remains poorly understood. To date, no research has explored the association between VAT metabolism and the expression of Her-2 or Ki-67 in GC, and their correlation remains unclear. A single animal study indicated that increased expression of Ki-67 in intramuscular fat can stimulate macrophage proliferation in VAT, with cytokines secreted by macrophages potentially promoting insulin resistance (Amano et al, 2014). Nevertheless, insulin resistance may result in reduced cellular glucose metabolism as evidenced by decreased uptake on ^{18}F-FDG PET/CT imaging (Yoo et al, 2018).

Table 3. Predictive model performance for Ki-67 and Her-2.

	Ki-67		Her-2	
	LR	SVM	LR	SVM
Accuracy (SD)	0.79 (0.11)	0.69 (0.03)	0.86 (0.05)	0.85 (0.03)
AUC (SD)	0.86 (0.07)	0.83 (0.09)	0.84 (0.11)	0.65 (0.14)
Sensitivity (SD)	0.83 (0.09)	0.99 (0.01)	0.30 (0.27)	0.06 (0.13)
Specificity (SD)	0.72 (0.18)	0.18 (0.20)	0.86 (0.22)	0.90 (0.22)

SD, standard deviation; AUC, the area under of the receiver operator characteristic curve; Her-2, human epidermal growth factor receptor 2; LR, logistic regression; SVM, support vector machine.

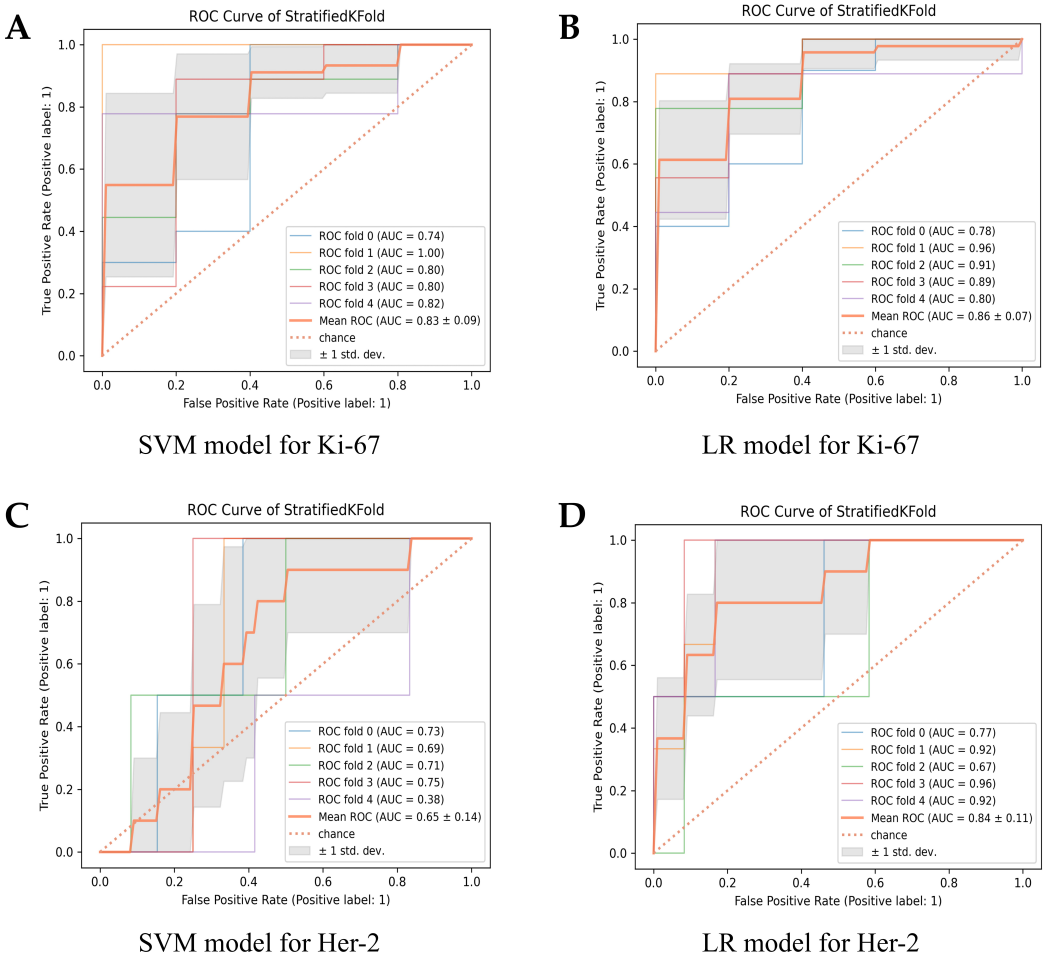

SVM model for Ki-67 | LR model for Ki-67

SVM model for Her-2 | LR model for Her-2

Fig. 4. Performance of the model for each task. (A,B) AUC for the SVM and LR models in predicting Ki-67 expression. (C,D) AUC for the SVM and LR models in predicting Her-2 expression.

Significant progress has been made in radiomics studies of Her-2 and Ki-67 in breast cancer and lung cancer. In the field of tumor imaging, ML technology is mainly applied in two categories: radiomics and convolutional neural networks. However, it is important to note that convolutional neural networks are susceptible to overfitting when used for disease classification predictions with a small sample size, leading to poor generalization ability of the model. Therefore, in our study,

Table 4. Predictive model performance for Ki-67 and Her-2.

	Features	R/H	*p*
Her-2	wavelet-LHH_GLRLM_HGLRE	8.159	0.004
	original_GLSZM_SZNN	4.014	0.045
	wavelet-LHH_GLDM_HGLE	8.797	0.003
	wavelet-LHH_GLDM_LGLE	8.797	0.003
Ki-67	waveletHHH_GLDM_GLV	4.139	0.042

GLRLM, Gray Level Run Length Matrix; GLSZM, Gray Level Size Zone Matrix; GLDM, Gray Level Dependence Matrix; HGLRE, High Gray Level Run Emphasis; SZNN, Size-Zone Non-Uniformity Normalized; HGLE, High Gray Level Emphasis; LGLE, Low Gray Level Emphasis; GLV, Gray Level Variance.

we utilized radiomics to construct the model due to its relatively low sample size limit and better performance of the model.

A previous study (Wang et al, 2021b) developed an RFE model to predict Her-2 expression by used CT images from 132 GC patients. The model was constructed using radiomics features extracted from arterial-phase and venous phase CT images. The results showed that the arterial phase-based radiomics model achieved the best performance, with AUC values of 0.756 in the training set and 0.83 in the test set. Wang et al (2021a) conducted a retrospective analysis of 101 patients with adenocarcinoma of the esophagogastric junction, identifying seven optimal features based on portal-phase CT images. The nomogram incorporating these best features, along with T-staging from CT, exhibited excellent predictive performance for Her-2 status (AUC, 0.946 in the training set and 0.903 in the test set).

Compared to CT, ^{18}F-FDG PET/CT is a non-invasive method that can provide *in vivo* metabolic activity of biological tissues. However, there are limited studies on radiomics based on ^{18}F-FDG PET/CT involving patients with GC. Jiang et al (2024) conducted a study with 118 patients with GC and established three models, namely LR, SVM, and RF, by extracting features from PET and CT images. Ultimately, the LR and RF models demonstrated good performance in predicting Her-2 expression status (Jiang et al, 2024). Liu et al (2023) extracted additional features from the same images, including Laplacian of Gaussian (LoG)-filtered features and wavelet-filtered features. They constructed an ensemble of multiple base (Adaboost) classifiers by combining these image features with clinical features. The accuracy of this model was 0.83, with a sensitivity of 0.846, specificity of 0.8, and AUC of 0.722 (Liu et al, 2023). Qin et al (2024) included 133 patients with GC and developed 6 XGBoost models based on CT and PET features combined with clinical features. The comprehensive model integrated 7 clinical features, 1 CT feature, and 5 PET features which demonstrated AUC values of 0.95 in the training cohort and an AUC value of 0.76 in the validation cohort. The nomogram of the model exhibited a superior net benefit on decision curve analysis and demonstrated good alignment agreement with observed values on the calibration curve (Qin et al, 2024).

Our study is the first research utilizing ML models based on VAT's ^{18}F-FDG images. In this study we trained the LR and SVM model based on VAT's glucose metabolism to predict the Ki-67 proliferation index of >50% and Her-2-positive expression. Additionally, we used five-fold cross-validation to enhance the robustness of the results obtained. The results indicate that the predictive models based on ^{18}F-FDG demonstrate strong effectiveness, and have potential value in clinical use. The maximum AUC for prediction of Ki-67 expression was 0.86, and the minimum AUC was 0.83, For prediction of Her-2 state, the highest AUC achieved was 0.84, while the lowest was 0.65. All the prediction models exhibit excellent accuracy, and the LR model of Her-2 expression has the highest accuracy. Whereas previous studies were based on tumor features, our research focused on extracting features of VAT, and achieved impressive performance. In contrast, it can be observed that the AUC of the LR model based on VAT in our study is much higher. However, our study only analyzed the PET features of VAT and did not include CT features or clinical features, which is a limitation of this research. A previous study reported that the model established using PET features alone had lower predictive efficacy for Her-2 expression status compared to the model established using CT features alone (Qin et al, 2024). This result can be reasonably explained by the higher spatial resolution of CT images compared to PET. However, as PET imaging is a functional metabolic imaging modality, it cannot achieve the high spatial resolution provided by CT images. Considering that the threshold range for VAT is relatively narrow and our main focus was on studying fat metabolism, we chose to exclude CT images when establishing the model and only used PET features. In both Qin et al (2024) and Liu et al (2023) studies on Her-2 expression status, clinical features did not enter into the final models. However, in Qin et al (2024) study, clinical features contributed value to the final model. Unfortunately, we did not include clinical characteristics in our research, and these may have contributed to the final outcome. In conclusion, our study has revealed the correlation between PET features of VAT and the expression of Her-2 or Ki-67 in GC.

As demonstrated by our findings, the features ultimately selected in all models are primarily derived from wavelet transform. This is consistent with previous research, indicating that wavelet features have greater value for the final model. The higher-order statistical features can better capture potential changes in the reaction tissue. Wavelet features are computed following the wavelet transform of the original image, which effectively reduces noise, sharpens the image, and enhances the most diagnostic information within the image (Ji et al, 2021).

In addition, the correlation between the radiological parameters such as PET semi-quantitative parameters, CT attenuation value and the selected optimal radiomics features with Ki-67 and Her-2 was analyzed. One radiomics feature was related to Ki-67, and 5 radiomics features were related to Her-2. Previous studies have analyzed the correlation between SUVmax and Her-2 expression, but the results are inconsistent. For example, Chen et al (2016) found that there was no significant correlation between SUVmax and Her-2 expression in GC. After excluding signet ring cell carcinoma, SUVmax of Her-2 negative group was significantly higher than that of Her-2 positive group (Chen et al, 2016). Zhang et al (2023) sug-

gests that the SUVmax of the Her-2 negative group was significantly higher than that of the Her-2 positive group ($p < 0.01$). Whereas Park et al (2018) conclusions obtained opposite conclusion (Park et al, 2018). A previous study found that the primary tumor SUVmax positively related to the expression of Ki-67 (Zhang et al, 2023). In our study, SUVmax is not correlated with Ki-67, but radiomics features are correlated with it, in addition, the radiomics features of VAT are also related to Her-2.

GLRLM quantifies the length in number of consecutive pixels on the same gray level value. High Gray Level Run Emphasis (HGLRE) measures the distribution of the higher gray-level values, with a higher value indicating a greater concentration of high gray-level values in the image and coarser structural textures. GLDM measures a number of connected voxels within a certain distance that are dependent on the center voxel; Gray Level Variance (GLV) indicates the variance in grey level in the image; Low Gray Level Emphasis (LGLE) measures the distribution of low gray-level values; High Gray Level Emphasis (HGLE) measures the distribution of low gray-level values, with a higher value indicating a greater concentration of gray-level values in the image; GLSZM quantifies a number of connected voxels that share the same gray level intensity; and Size-Zone Non-Uniformity Normalized (SZNN) measures the variability of size zone volumes throughout the image, with a lower value indicating more homogeneity among zone size volumes in the image.

For now, the biological significance of radiometric features, and their utility for predicting the clinical outcome and prognosis of patients, remain unclear (Tomaszewski and Gillies, 2021), but our results indicate that the expression of Ki-67 and Her-2 state can be predicted using a non-invasive method-metabolic radiomics features of VAT. The underlying relationship between FDG metabolic changes in VAT and the expression of Ki-67 and Her-2 remains to be elucidated.

Our preliminary studies have demonstrated that ^{18}F-FDG PET/CT metabolic features of VAT in GC patients correlate with tumor immunohistochemical markers; these results can provide further information on tumor proliferation and related biological behavior before aggressive examination. In addition, in the 2 models developed in this study, different models showed different prediction performance, indicating that the choice of different feature screening combined with classifier model type has an important impact on the results. Our results can provide clinical guidance for the radiological assessment of Ki-67 and its Her-2 and subsequent treatment decisions.

This study also has several limitations. Firstly, thresholding combined with manual segmentation was used in this study, which is considered as the gold standard. Although we used manual segmentation to eliminate the influence of intestinal physiological hypermetabolism on the results, this method has significant inter-reader bias and is time-consuming and labor-intensive. Secondly, there is no consensus on the threshold range of fat, and different devices and different parameter adjustments of the device will affect the threshold range of fat. Third, this is a retrospective case-control study, instead of a randomized controlled trial. Therefore, there is still some risk of bias. Fourth, this study was a single-center clinical trial.

The sample size is small and there is no validation set. Fifth, as this was a small sample study, we did not explore the contribution value of VAT to the differentiation of highly differentiated and adherent adenocarcinoma with hypometabolism.

Conclusion

In summary, the present study developed a ML model of ^{18}F-FDG PET metabolism, using the ^{18}F-FDG radiomics features of VAT to predict the expression of Ki-67 and Her-2 in GC. These results indicate that there is a correlation between the metabolomic features of VAT and the expression of Ki-67 and Her-2. It demonstrates the feasibility of applying radiomics features of VAT to provide non-invasive personalized prediction information for GC patients to supplement conventional clinical decision-making methods. Based on the limitations of this study, additional data from multi-center prospective studies will be included in the future, since multi-center validation is needed. Future studies may also add different ML and deep learning models, and measure VAT with different radiological images, such as CT and MRI.

Key Points

- Used the ^{18}F-FDG PET/CT radiomics features of VAT combined with ML to predict Her-2 and Ki-67 status in GC.
- The logistic regression (LR) model for Ki-67 displayed the highest diagnostic performance.
- The metabolism of VAT is intrinsically associated with expression of Ki-67 and Her-2, and this association can be assessed using ^{18}F-FDG PET/CT.

Availability of Data and Materials

The raw data supporting the conclusions of this article will be made available by the authors if required, without undue reservation.

Author Contributions

DC, BL and RZ designed the research. DC and BL performed the research. RZ provided help and advice on the experiments. DC analyzed the data. DC drafted the manuscript. All authors contributed to important editorial changes of important content in the manuscript. All authors read and approved the final manuscript. All authors have participated sufficiently in the work and agreed to be accountable for all aspects of the work.

Ethics Approval and Consent to Participate

This study was conducted in accordance with the Declaration of Helsinki and approved by the Medical Ethics Committee of Chongqing University Cancer Hospi-

tal (ethics number: CZLS2024006-A). The Medical Ethics Committee of Chongqing University Cancer Hospital waived the need for informed consent.

Acknowledgement

Not applicable.

Funding

This research was funded by the Technology Innovation and Application Development Project of Shapingba District of Chongqing Municipality (grant numbers 202397 and 202396).

Conflict of Interest

The authors declare no conflict of interest.

References

Abrahao-Machado LF, Scapulatempo-Neto C. HER2 testing in gastric cancer: An update. World Journal of Gastroenterology. 2016; 22: 4619–4625. https://doi.org/10.3748/wjg.v22.i19.4619

Acar E, Turgut B, Yiğit S, Kaya G. Comparison of the volumetric and radiomics findings of 18F-FDG PET/CT images with immunohistochemical prognostic factors in local/locally advanced breast cancer. Nuclear Medicine Communications. 2019; 40: 764–772. https://doi.org/10.1097/MNM.0000000000001019

Amano SU, Cohen JL, Vangala P, Tencerova M, Nicoloro SM, Yawe JC, et al. Local proliferation of macrophages contributes to obesity-associated adipose tissue inflammation. Cell Metabolism. 2014; 19: 162–171. https://doi.org/10.1016/j.cmet.2013.11.017

Avgerinos KI, Spyrou N, Mantzoros CS, Dalamaga M. Obesity and cancer risk: Emerging biological mechanisms and perspectives. Metabolism: Clinical and Experimental. 2019; 92: 121–135. https://doi.org/10.1016/j.metabol.2018.11.001

Awadh M, Darwish A, Alqatari H, Buzaid FM, Darwish A. A descriptive analysis of gastric cancer with an immunohistochemical Study of Ki67 and p53 as prognostic factors.: Bahrain experience. Saudi Medical Journal. 2023; 44: 1300–1309. https://doi.org/10.15537/smj.2023.44.12.20230246

Boku N. HER2-positive gastric cancer. Gastric Cancer. 2014; 17: 1–12. https://doi.org/10.1007/s10120-013-0252-z

Bray F, Laversanne M, Sung H, Ferlay J, Siegel RL, Soerjomataram I, et al. Global cancer statistics 2022: GLOBOCAN estimates of incidence and mortality worldwide for 36 cancers in 185 countries. CA: A Cancer Journal for Clinicians. 2024; 74: 229–263. https://doi.org/10.3322/caac.21834

Chen R, Zhou X, Liu J, Huang G. Relationship Between 18F-FDG PET/CT Findings and HER2 Expression in Gastric Cancer. Journal of Nuclear Medicine. 2016; 57: 1040–1044. https://doi.org/10.2967/jnumed.115.171165

Dondi F, Albano D, Giubbini R, Bertagna F. 18F-FDG PET and PET/CT for the evaluation of gastric signet ring cell carcinoma: a systematic review. Nuclear Medicine Communications. 2021; 42: 1293–1300. https://doi.org/10.1097/MNM.0000000000001481

Ji B, Hosseini Z, Wang L, Zhou L, Tu X, Mao H. Spectral Wavelet-feature Analysis and Classification Assisted Denoising for enhancing magnetic resonance spectroscopy. NMR in Biomedicine. 2021; 34: e4497. https://doi.org/10.1002/nbm.4497

Jiang X, Li T, Wang J, Zhang Z, Chen X, Zhang J, et al. Noninvasive Assessment of HER2 Expression Status in Gastric Cancer Using 18F-FDG Positron Emission Tomography/Computed Tomography-

Based Radiomics: A Pilot Study. Cancer Biotherapy & Radiopharmaceuticals. 2024; 39: 169–177. https://doi.org/10.1089/cbr.2023.0162

Le Berre C, Sandborn WJ, Aridhi S, Devignes MD, Fournier L, Smaïl-Tabbone M, et al. Application of Artificial Intelligence to Gastroenterology and Hepatology. Gastroenterology. 2020; 158: 76–94.e2. https://doi.org/10.1053/j.gastro.2019.08.058

Lee JW, Son MW, Chung IK, Cho YS, Lee MS, Lee SM. Significance of CT attenuation and F-18 fluorodeoxyglucose uptake of visceral adipose tissue for predicting survival in gastric cancer patients after curative surgical resection. Gastric Cancer. 2020; 23: 273–284. https://doi.org/10.1007/s10120-019-01001-2

Levy I, Gralnek IM. Complications of diagnostic colonoscopy, upper endoscopy, and enteroscopy. Best Practice & Research. Clinical Gastroenterology. 2016; 30: 705–718. https://doi.org/10.1016/j.bpg.2016.09.005

Li LT, Jiang G, Chen Q, Zheng JN. Ki67 is a promising molecular target in the diagnosis of cancer (review). Molecular Medicine Reports. 2015; 11: 1566–1572. https://doi.org/10.3892/mmr.2014.2914

Liu Q, Li J, Xin B, Sun Y, Wang X, Song S. Preoperative 18F-FDG PET/CT radiomics analysis for predicting HER2 expression and prognosis in gastric cancer. Quantitative Imaging in Medicine and Surgery. 2023; 13: 1537–1549. https://doi.org/10.21037/qims-22-148

Lu J, Xue Z, Xie JG, Xu BB, Yang HB, Wu D, et al. Preoperative Muscle-Adipose Index: A New Prognostic Factor for Gastric Cancer. Annals of Surgical Oncology. 2022; 29: 4595–4607. https://doi.org/10.1245/s10434-022-11509-0

Ma T, Cui J, Wang L, Li H, Ye Z, Gao X. A multiphase contrast-enhanced CT radiomics model for prediction of human epidermal growth factor receptor 2 status in advanced gastric cancer. Frontiers in Genetics. 2022a; 13: 968027. https://doi.org/10.3389/fgene.2022.968027

Ma T, Li X, Zhang T, Duan M, Ma Q, Cong L, et al. Effect of visceral adipose tissue on the accuracy of preoperative T-staging of gastric cancer. European Journal of Radiology. 2022b; 155: 110488. https://doi.org/10.1016/j.ejrad.2022.110488

Martin-Perez M, Urdiroz-Urricelqui U, Bigas C, Benitah SA. The role of lipids in cancer progression and metastasis. Cell Metabolism. 2022; 34: 1675–1699. https://doi.org/10.1016/j.cmet.2022.09.023

Matsui R, Inaki N, Tsuji T. Impact of visceral adipose tissue on long-term outcomes after gastrectomy for advanced gastric cancer. Nutrition. 2022; 97: 111619. https://doi.org/10.1016/j.nut.2022.111619

Moon CM, Lee YY, Kim DY, Yoon W, Baek BH, Park JH, et al. Preoperative prediction of Ki-67 and p53 status in meningioma using a multiparametric MRI-based clinical-radiomic model. Frontiers in Oncology. 2023; 13: 1138069. https://doi.org/10.3389/fonc.2023.1138069

Orășeanu A, Brisc MC, Maghiar OA, Popa H, Brisc CM, Șolea SF, et al. Landscape of Innovative Methods for Early Diagnosis of Gastric Cancer: A Systematic Review. Diagnostics. 2023; 13: 3608. https://doi.org/10.3390/diagnostics13243608

Pan F, Feng L, Liu B, Hu Y, Wang Q. Application of radiomics in diagnosis and treatment of lung cancer. Frontiers in Pharmacology. 2023; 14: 1295511. https://doi.org/10.3389/fphar.2023.1295511

Park JS, Lee N, Beom SH, Kim HS, Lee CK, Rha SY, et al. The prognostic value of volume-based parameters using 18F-FDG PET/CT in gastric cancer according to HER2 status. Gastric Cancer. 2018; 21: 213–224. https://doi.org/10.1007/s10120-017-0739-0

Qin L, Chen W, Ye Y, Yi H, Pang W, Long B, et al. Prediction of HER2 Expression in Gastric Adenocarcinoma Based On Preoperative Noninvasive Multimodal 18F-FDG PET/CT Imaging. Academic Radiology. 2024. (online ahead of print) https://doi.org/10.1016/j.acra.2024.01.022

Roviello G, Catalano M, Iannone LF, Marano L, Brugia M, Rossi G, et al. Current status and future perspectives in HER2 positive advanced gastric cancer. Clinical & Translational Oncology. 2022; 24: 981–996. https://doi.org/10.1007/s12094-021-02760-0

Smyth EC, Nilsson M, Grabsch HI, van Grieken NC, Lordick F. Gastric cancer. Lancet. 2020; 396: 635–648. https://doi.org/10.1016/S0140-6736(20)31288-5

Tomaszewski MR, Gillies RJ. The Biological Meaning of Radiomic Features. Radiology. 2021; 299: E256. https://doi.org/10.1148/radiol.2021219005

Tunali I, Gillies RJ, Schabath MB. Application of Radiomics and Artificial Intelligence for Lung Cancer Precision Medicine. Cold Spring Harbor Perspectives in Medicine. 2021; 11: a039537. https://doi.org/10.1101/cshperspect.a039537

Wang S, Chen Y, Zhang H, Liang Z, Bu J. The Value of Predicting Human Epidermal Growth Factor Receptor 2 Status in Adenocarcinoma of the Esophagogastric Junction on CT-Based Radiomics Nomogram. Frontiers in Oncology. 2021a; 11: 707686. https://doi.org/10.3389/fonc.2021.707686

Wang Y, Yu Y, Han W, Zhang YJ, Jiang L, Xue HD, et al. CT Radiomics for Distinction of Human Epidermal Growth Factor Receptor 2 Negative Gastric Cancer. Academic Radiology. 2021b; 28: e86–e92. https://doi.org/10.1016/j.acra.2020.02.018

Yoo ID, Lee SM, Lee JW, Baek MJ, Ahn TS. Usefulness of metabolic activity of adipose tissue in FDG PET/CT of colorectal cancer. Abdominal Radiology. 2018; 43: 2052–2059. https://doi.org/10.1007/s00261-017-1418-7

Zhang LF, Li JL, Wang YH, Tai XH, Liu L, Zhang XX, et al. The Correlation Between 18F-Fluorodeoxyglucose-Positron Emission Tomography/Computed Tomography Semiquantitative Parameters and the Clinical Features and Pathological Biological Indexes of Gastric Cancer. Cancer Biotherapy & Radiopharmaceuticals. 2023; 38: 364–370. https://doi.org/10.1089/cbr.2020.4150

Zhao H, Liang P, Yong L, Cheng M, Zhang Y, Huang M, et al. Development and external validation of a radiomics model for assessment of HER2 positivity in men and women presenting with gastric cancer. Insights into Imaging. 2023; 14: 20. https://doi.org/10.1186/s13244-022-01361-x